Supporting Information

The OH Radical-Initiated Single-Electron Transfer for Accelerated Degradation via Carbocation Intermediates

Xiyang Ge, Yiyan Yin, Jianghui Sun, Jin Ouyang, Na Na*

Key Laboratory of Radiopharmaceuticals, Ministry of Education, College of Chemistry, Beijing Normal University, Beijing 100875, China

*Corresponding Authors

Email：nana@bnu.edu.cn

Contents

Experimental Procedures

Chemicals All reagents and solvents were purchased from commercial sources and used without further purification. Manganese sulfate monohydrate ($MnSO_4 \cdot H_2O$), sodium persulfate ($Na_2S_2O_8$), 3,3',5,5'-Tetramethylbenzidine (TMB) and hydroxychloroquine sulfate (HCQ) were purchased from Innochem. (Beijing, China). Methanol and Isopropyl alcohol of HPLC grade were purchased from Fisher Chemical (USA). Deionized water (Mill-Q, Millipore, 18.2 MΩ) was used in all experiments.

Mass spectrometry On-line monitoring was performed on an LTQ XL (Thermo Fisher Scientific, USA) instrument using a homemade ionization source of ESSI-MS. The operational parameters were as follows: full-scan positive (+) ion spectra were obtained over the m/z range from 50 to 500; the temperature of the MS inlet capillary was 250 °C; the capillary voltage and tube lens voltage were set to 100 V and 120 V, respectively. The maximum ion injection time was 1000 ms. In addition, 5kV high voltage was added to the solution. All MS results were obtained and processed using the Xcalibur or Microcal Origin (version 8.0) software. High-resolution mass spectrometry was conducted using a Triple TOF 5600+ (AB SCIEX, USA). The mass spectrometer was equipped with a heated electrospray ionization (HESI) source. Analyses were carried out in positive mode.

Other instruments Transmission electron microscopy (TEM) imaging was performed on an FEI Talos 200S transmission electron microscope with an operating voltage of 200 kV. Field emission scanning electron microscopy (FESEM) was carried on the S-8010 (Hitachi, Japan). UV–vis absorbed spectra was measured by a UV 2600 spectrophotometer (Shimadzu, Japan). FLS980 fluorescence spectrophotometer (Edinburgh Instruments, UK). X-ray diffraction measurements were performed with a Maxima XRD-7000 (Shimadzu, Japan). The XPS spectra were recorded using a PHI-5300 ESCA spectrometer (Perkin Elmer) equipped with an Al Kα excitation source. Electron Paramagnetic Resonance (EPR) spectra were collected with a Brucker ER200-SRC-10/12 spectrometer. Raman spectra were recorded at room temperature using a Raman spectrometer (Renishaw RM-1000) in a back-scattering

geometry with a 532 nm laser as the excitation source. Fourier transform infrared (FT-IR) spectra of the samples were analyzed on a Perkin-Elmer TGA 7 infrared spectrometer to identify the functional groups on the surface of all samples.

Synthesis of β-MnO_2 9.5 mmol of $MnSO_4 \cdot H_2O$ and 9.5 mmol of $Na_2S_2O_8$ were mixed in 70 mL of distilled water for well stirring. The solution was then transferred into a stainless-steel autoclave and heated at 90 °C for 24 h. The solution was collected after each cycle by filtration, washed with water and ethanol, and then dried in a vacuum oven. The black solid was calcinated at 350 °C for 3 h in an air atmosphere to obtain β-MnO_2 nanorods [1].

Degradation Measurement 10mg β-MnO_2 was directly added to the HCQ solution to 1 uM HCQ solution and dispersed evenly by ultrasound. Under the condition of stirring, the air plasma was passed into the MnO_2 mixed solution, and the solution formed electrospray into the mass spectrum by a capillary injection device. At the same time, the air plasma was passed into the HCQ solution without MnO_2 to compare the influence of catalyst. In the comparison experiment, the conditions of the plasma system without MnO_2 reaction were the same as above. To study the active species, without changing other experimental conditions, excess TMB and isopropanol were added immediately after adding the plasma into the HCQ solution with MnO_2, respectively.

Computational procedure Quantum chemical calculations were performed using density functional theory (DFT) with the Gaussian 09 program package [2]. The geometrical parameters of reactants, intermediates (IM), transition states (TS), and products were optimized at the M06-2X/DEF2TZVP level. Vibrational frequencies were computed analytically at the same level of theory to correct for zero-point energy (ZPE) and confirm whether the structures are minima (no imaginary frequencies) or transition states (only one imaginary frequency). The transition state was also verified with the intrinsic reaction

coordinate (IRC) calculations. Moreover, the solvent effect was evaluated by using water as the solvent. The condensed electrostatic potential (ESP) mapped molecular surface was obtained by the Multiwfn program. The Fukui function was introduced to describe the nucleophilic, electrophilic, and radical attacks. The simplified Fukui function corresponding to the above three situations are as follows:

Nucleophilic attack: $f^{+}(r) = \rho_{N+1}(r) - \rho_{N}(r)$ (1)

Electrophilic attack: $f^{-}(r) = \rho_{N}(r) - \rho_{N-1}(r)$ (2)

Radical attack: $f^{0}(r) = [f^{+}(r) + f^{-}(r)]/2 = [\rho_{N+1}(r) - \rho_{N-1}(r)]/2$ (3)

where $\rho_{N+1}(r)$, $\rho_{N+1}(r)$ and $\rho_{N-1}(r)$ are the electronic densities of the system with N+1, N and N-1 electrons, respectively. And the nucleophilic, electrophilic and radical attacks were evaluated by Eqs. (1) - (3), respectively. In this article, all electronic structures were analyzed by Multiwfn software [3].

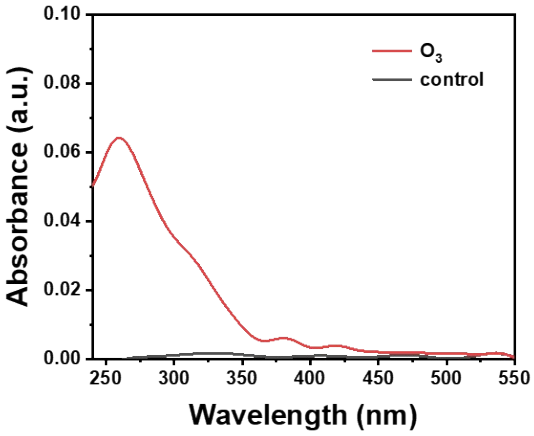

Figure S1 The UV-vis absorption of plasma-treated water. The absorption at about 254 nm indicated the presence of O_3.

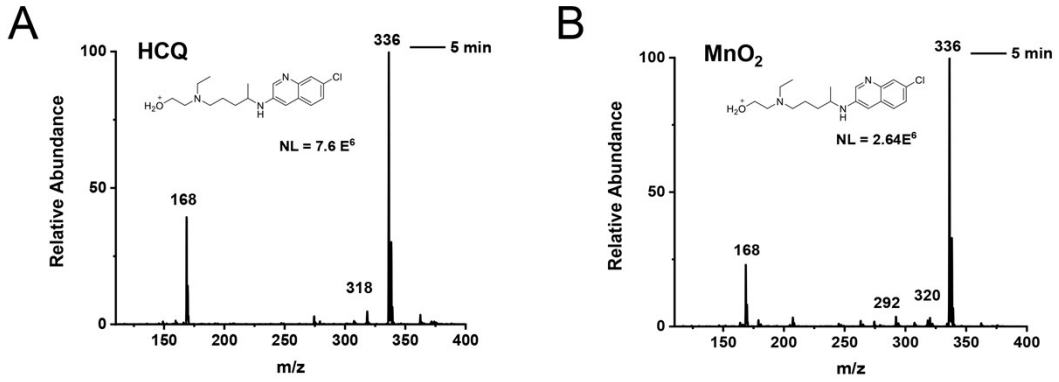

Figure S2 Mass spectra of reaction intermediates in (A) HCQ system and (B) MnO_2 system at 5 min.

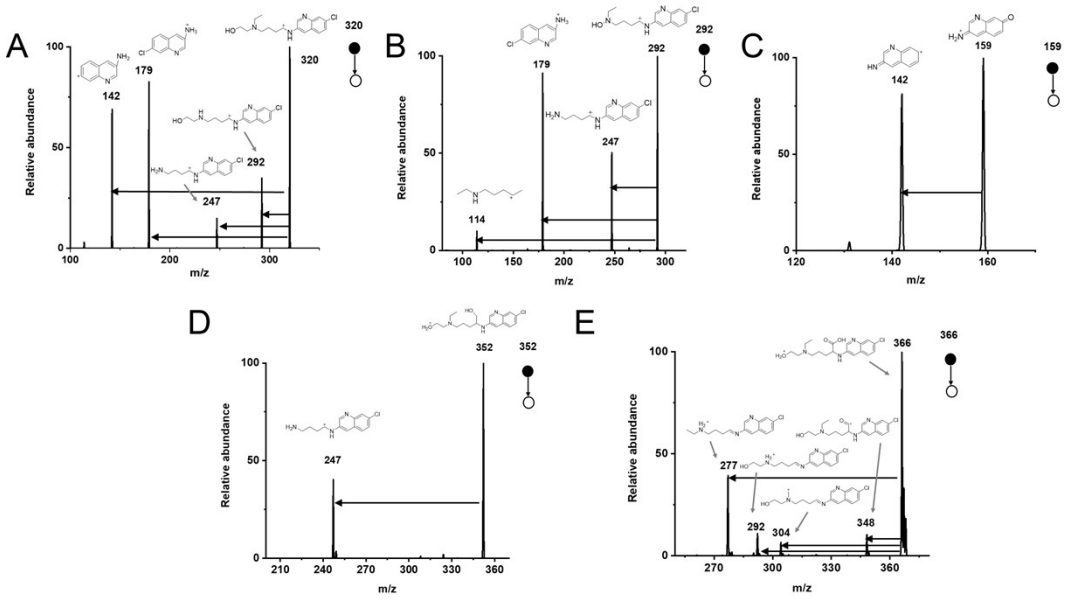

Figure S3 The CID diagram of ions (A) m/z 320; (B) m/z 292; (C) m/z 159; (D) m/z 352 and (E) m/z 366 in the MnO_2-plasma system.

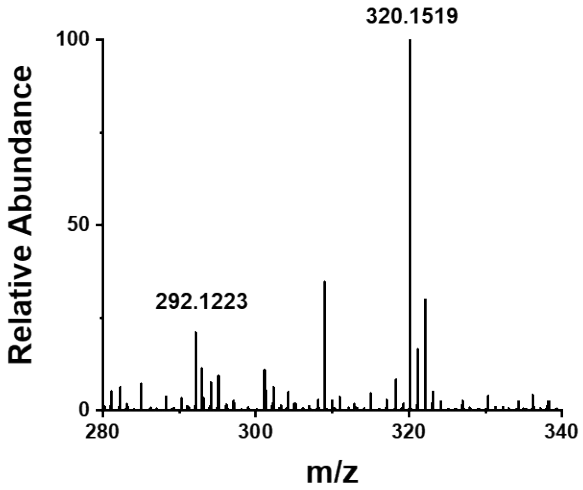

Figure S4 The high-resolution mass spectrometry (HR-MS) of carbocations.

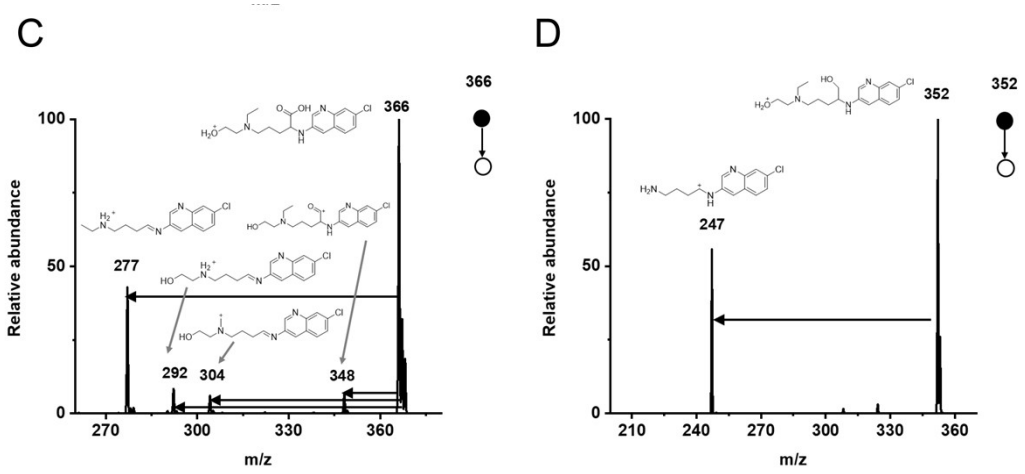

Figure S5 The CID diagram of ions (A) m/z 366 and (B) m/z 352 in the single plasma system.

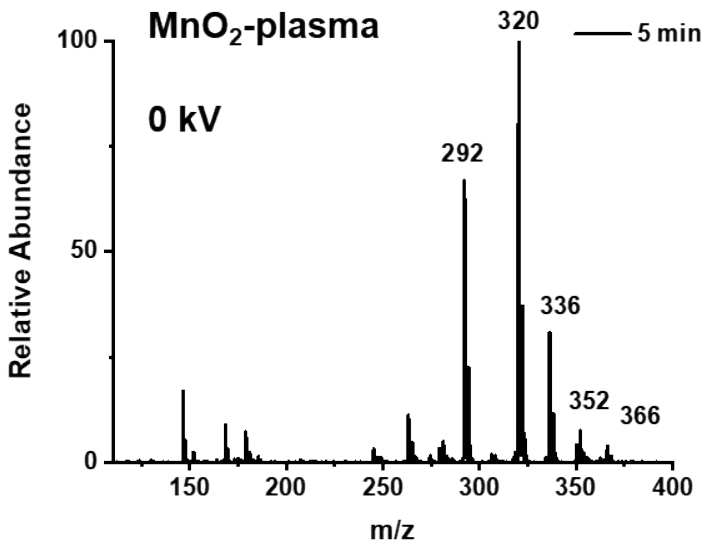

Figure S6 Mass spectra of reaction intermediates in the MnO_2-plasma system without high-voltage of ESSI applied on. Degradation: for 5 min.

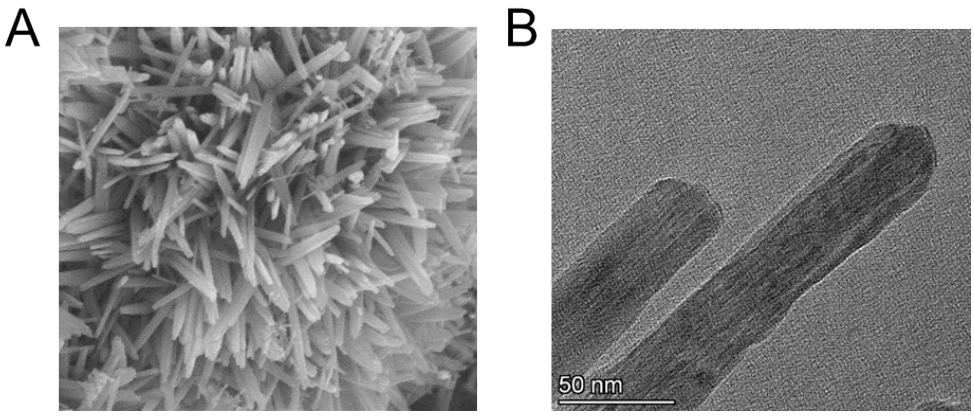

Figure S7 Structure of prepared MnO_2 nanorod. (A) SEM image and (B) TEM image.

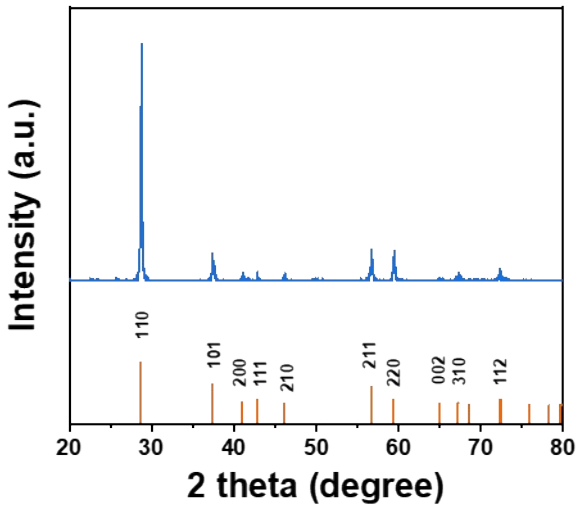

Figure S8 XRD pattern of β-MnO_2.

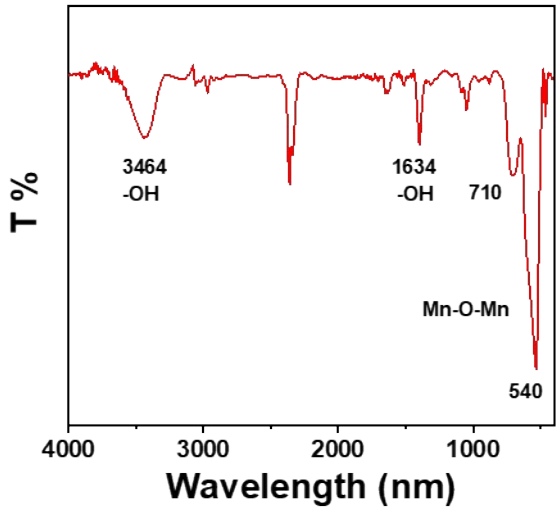

Figure S9FTIR spectrum of MnO_2.

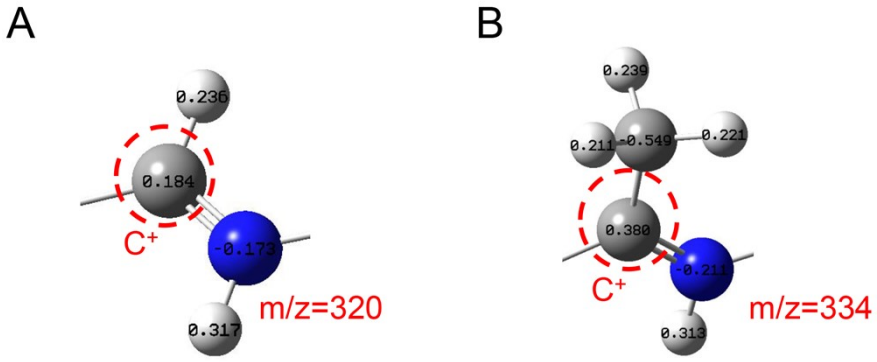

Figure S10 The charge distribution of C^+ in carbocations of C1 (m/z 320, A) and C1' (m/z 334, B).

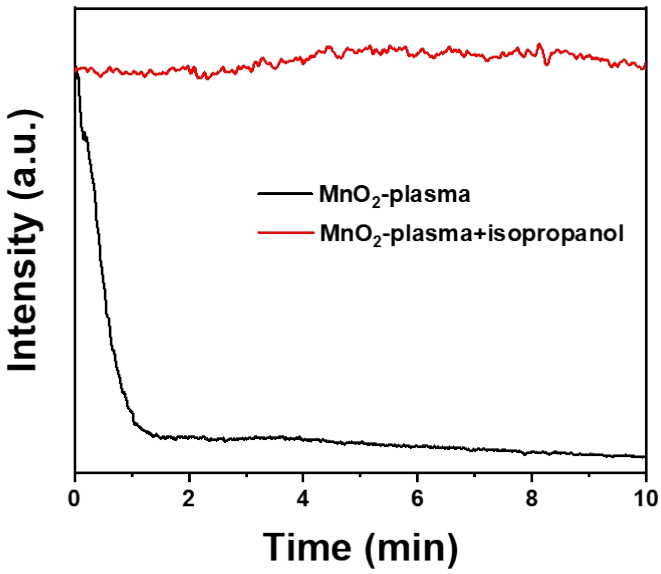

Figure S11 The on-line monitoring of $[HCQ + H]^+$ in the MnO_2-plasma with isopropanol and without isopropanol.

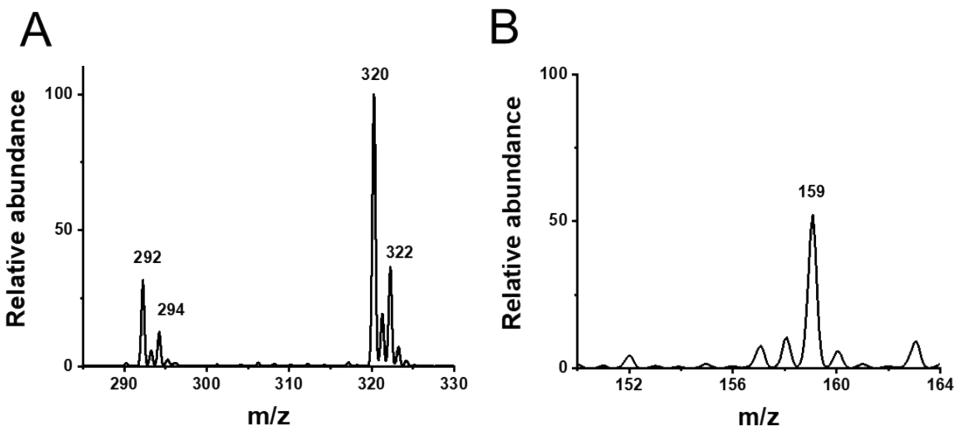

Figure S12 $[M+2]^+$ peaks of ions at m/z 320, 292 and 159.

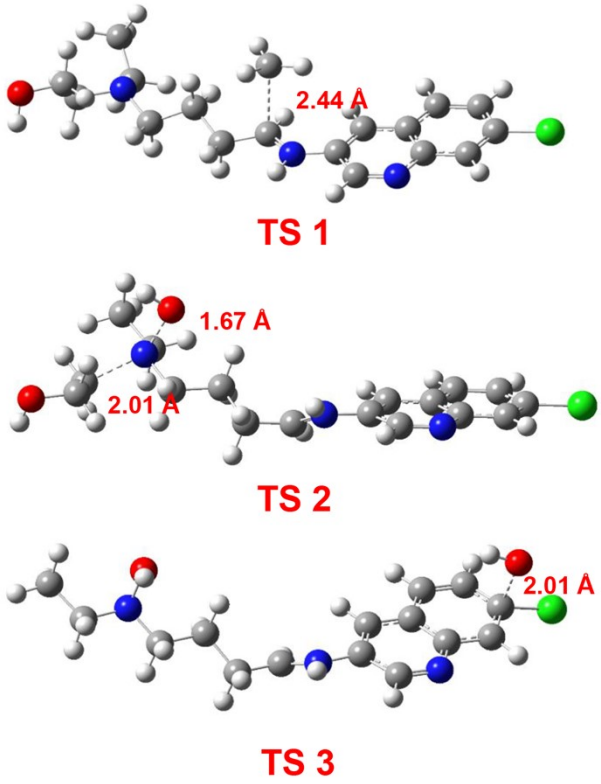

Figure S13 The transition states (TS) of the formation of the carbocations.

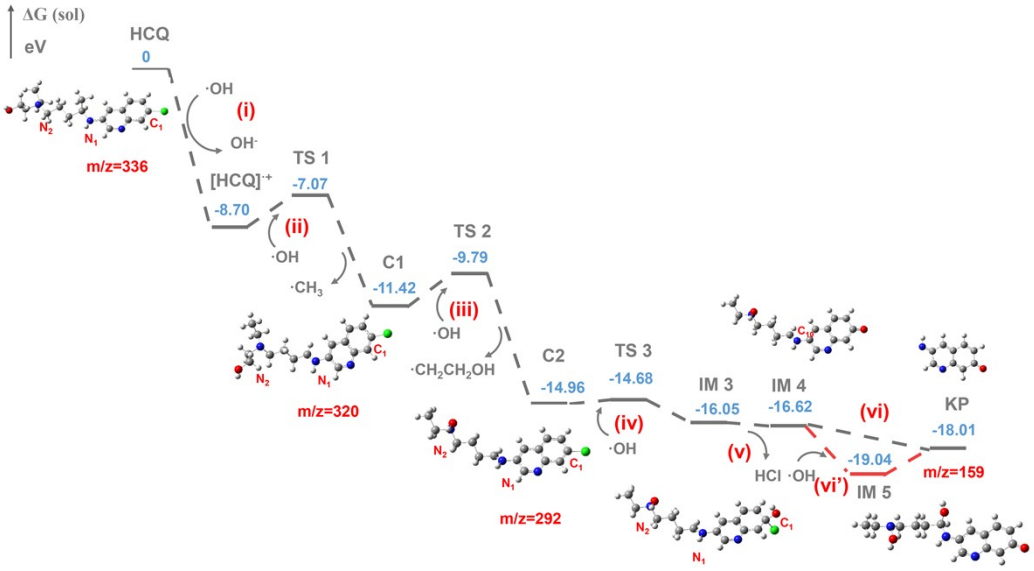

Figure S14 The energy diagram for the HCQ degradation.

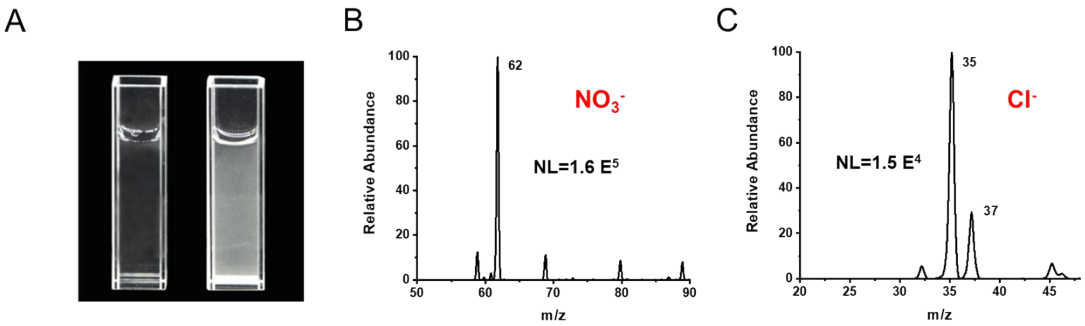

Figure S15 The examination on the final products of the advanced degradation. (A) The pictures of $Ca(OH)_2$ solutions (0.17 g/mL) before (left) and after (right) introducing gas products. MS spectra of NO_3^- (B) and Cl^- (C) recorded in the reaction solution after 1h of degradation.

Table S1 The carbocation intermediates with element composition and ppm error.

m/z	Calculated	Element Composition	Ppm error
3201519	320.1524	$C_{17}H_{23}N_3OCl$	-1.61
292.1223	292.1211	$C_{15}H_{19}N_3OCl$	4.05

Table S2 The Fukui function indices of HCQ.

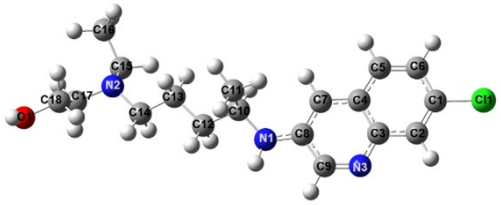

Atoms	Fukui Function Indices		
	$f+$	$f-$	$f0$
C_1	0.0386	0.0587	0.0486
C_2	0.0673	0.0327	0.0500
C_3	0.0127	0.0375	0.0251
C_4	0.0165	0.0225	0.0195
C_5	0.0669	0.0446	0.0558
C_6	0.0688	0.0323	0.0506
C_7	0.0724	0.0752	0.0738
C_8	0.0429	0.0464	0.0446
C_9	0.1061	0.0390	0.0726
C_{10}	0.0035	0.0086	0.0061
C_{11}	0.0067	0.0175	0.0121
C_{12}	0.003	0.0039	0.0035
C_{13}	0.0023	0.0039	0.0031
C_{14}	0.0015	0.0022	0.0019
C_{15}	0.0001	0.0004	0.0002
C_{16}	0.0021	0.0027	0.0024
C_{17}	0.0019	0.0024	0.0022
C_{18}	0.0004	0.0005	0.0005
N_1	0.0209	0.1202	0.0705
N_2	0.0002	0.0009	0.0006
Cl_1	0.0845	0.1112	0.0978
O_1	0.0044	0.0054	0.0049

Table S3 The Fukui function indices of C1.

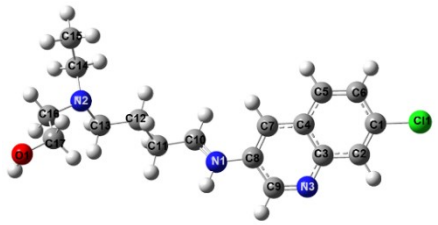

Atoms	Fukui Function Indices		
	$f+$	$f-$	$f0$
C_1	0.0321	0.0106	0.0214
C_2	0.0169	0.0065	0.0117
C_3	0.0271	0.0066	0.0169
C_4	0.0103	0.0028	0.0169
C_5	0.0193	0.0031	0.0112
C_6	0.0280	0.0089	0.0185
C_7	0.047	0.0016	0.0243
C_8	0.0011	-0.0039	-0.0014
C_9	0.0125	0.0028	0.0077
C_{10}	0.1872	-0.0137	0.0867
C_{11}	0.0244	0.0079	0.0161
C_{12}	0.0166	0.0077	0.0121
C_{13}	0.0085	0.0296	0.0191
C_{14}	0.0014	0.0358	0.0186
C_{15}	0.0045	0.0244	0.0144
C_{16}	0.0045	0.0343	0.0194
C_{17}	0.0011	0.0206	0.0108
N_1	0.1003	0.0137	0.0570
N_2	0.0031	0.2536	0.1284
Cl_1	0.0646	0.0271	0.0458
O_1	0.0108	0.0423	0.0266

REFERENCES

[1] R. Yang, et al., *Small*, 2021, **17**, 2102408.

[2] M.J. Frisch, Gaussian 09, 2009, Revision D.01. M. J. Frisch, G. W. Trucks, H. B. Schlegel, G. E. Scuseria, M. A. Robb, J. R. Cheeseman, G. Scalmani, V. Barone, B. Mennucci, G. A. Petersson, H. Nakatsuji, M. Caricato, X. Li, H. P. Hratchian, A. F. Izmaylov, J. Bloino, G. Zheng, J. L. Sonnenberg, M. Hada, M. Ehara, K. Toyota, R. Fukuda, J. Hasegawa, M. Ishida, T. Nakajima, Y. Honda, O. Kitao, H. Nakai, T. Vreven, J. A. Montgomery, J. E. Peralta, F. Ogliaro, M. Bearpark, J. J. Heyd, E. Brothers, K. N. Kudin, V. N. Staroverov, R. Kobayashi, J. Normand, K. Raghavachari, A. Rendell, J. C. Burant, S. S. Iyengar, J. Tomasi, M. Cossi, N. Rega, J. M. Millam, M. Klene, J. E. Knox, J. B. Cross, V. Bakken, C. Adamo, J. Jaramillo, R. Gomperts, R. E. Stratmann, O. Yazyev, A. J. Austin, R. Cammi, C. Pomelli, J. W. Ochterski, R. L. Martin, K. Morokuma, V. G. Zakrzewski, G. A. Voth, P. Salvador, J. J. Dannenberg, S. Dapprich, A. D. Daniels, Farkas, J. B. Foresman, J. V Ortiz, J. Cioslowski and D. J. Fox, Gaussian 09, Revision D.01, Gaussian Inc.; Wallingford, CT, 2009 .

[3] T. Lu, F. Chen, *J. Comput. Chem*., 2012, **33**, 580-592.